JMEPEG (2016) 25:1709–1721
DOI: 10.1007/s11665-016-2011-x

1059-9495/$19.00

FE Simulation Models for Hot Stamping an Automobile Component with Tailor-Welded High-Strength Steels

Bingtao Tang, Qiaoling Wang, Zhaohui Wei, Xianju Meng, and Zhengjun Yuan

(Submitted June 10, 2015; in revised form March 1, 2016; published online March 22, 2016)

Ultra-high-strength in sheet metal parts can be achieved with hot stamping process. To improve the crash performance and save vehicle weight, it is necessary to produce components with tailored properties. The use of tailor-welded high-strength steel is a relatively new hot stamping process for saving weight and obtaining desired local stiffness and crash performance. The simulation of hot stamping boron steel, especially tailor-welded blanks (TWBs) stamping, is more complex and challenging. Information about thermal/mechanical properties of tools and sheet materials, heat transfer, and friction between the deforming material and the tools is required in detail. In this study, the boron-manganese steel B1500HS and high-strength low-alloy steel B340LA are tailor welded and hot stamped. In order to precisely simulate the hot stamping process, modeling and simulation of hot stamping tailor-welded high-strength steels, including phase transformation modeling, thermal modeling, and thermal-mechanical modeling, is investigated. Meanwhile, the welding zone of tailor-welded blanks should be sufficiently accurate to describe thermal, mechanical, and metallurgical parameters. FE simulation model using TWBs with the thickness combination of 1.6 mm boron steel and 1.2 mm low-alloy steel is established. In order to evaluate the mechanical properties of the hot stamped automotive component (mini b-pillar), hardness and microstructure at each region are investigated. The comparisons between simulated results and experimental observations show the reliability of thermo-mechanical and metallurgical modeling strategies of TWBs hot stamping process.

Keywords boron steel, formability, hot stamping, phase transformation, tailor-welded blanks

1. Introduction

The hot stamping process gained increasing importance due to the increasing demand for automobile safety and lightweight requirements (Ref 1, 2). In order to reduce the assembly cost and maintain good ductility which is crucial for the crash performance in security-relevant components like the b-pillar, hot stamping of tailor-welded blanks, one of the new hot stamping processes, is now focused on supplying functionally optimized mechanical properties within a single component.

The concept of the partial heating strategy is used to develop the local mechanical properties in the heating step of hot stamping process (Ref 3, 4). Another strategy to produce components with localized mechanical properties is controlling cooling rate during the quenching process. Heated tools are used to decrease the cooling rate, producing a more ductile microstructure with lower strength (Ref 5, 6). Tool materials with different thermal conductivities are used to control cooling rate and thus the mechanical properties of the stamped part (Ref 7). Similarly, ceramic insulation plates in the flange area of a hot stamping tool are used to supply low-conductivity tool segments (Ref 8).

Abbreviations	
TWBs	Tailor-welded blanks
HSLA	High-strength low-alloy
HAZ	Heat-affected zone
JMA	Johnson-Mehl-Avrami
TTT	Time-temperature transformation
FLDs	Forming limit diagrams
FLCs	Forming limit curves

One component can meet the same requirements as the one with several components tailor welded together, providing both weight- and structure-optimized components. In order to find a complementary material to the boron steel 22MnB5, Stopp et al. (Ref 9) and Lamprecht (Ref 10) have conducted numerous experiments with several different steel grades. In Ref 11, Lechler et al. pointed out that the micro-alloyed steel HX340LAD was an appropriate joining partner. The material HX340LA combined with boron steel 22MnB5 can supply components with expected tensile strength distribution. Tang et al. (Ref 12) have conducted basic experiments on microhardness and metallography on different base materials and corresponding weld seams. They pointed out that the B340LA steel was an appropriate joint partner to boron steel B1500HS with ideal thermal and mechanical properties. In addition to the characterization of the basic materials, special emphasis should be placed on the modeling and simulation of hot stamping tailor-welded high-strength steels. Till now, there are only few reports on finite element simulation models of hot stamping using tailor-welded high-strength steels.

Bingtao Tang and **Qiaoling Wang**, School of Material Science and Engineering, Shandong Jianzhu University, Fengming Rd, Lingang Development Zone, Jinan, China; **Zhaohui Wei**, School of Material Science and Engineering, Fujian University of Technology, Xueyuan Rd, University Town, Fuzhou, Minhou, China; and **Xianju Meng** and **Zhengjun Yuan**, School of Mechanical and Electrical Engineering, Shandong Jianzhu University, Fengming Rd, Lingang Development Zone, Jinan, China. Contact e-mail: tbtsh@hotmail.com.

During the hot stamping process, the workpiece is initially heated to austenitization temperature and subsequently cooled down to room temperature by heat transfer to the contacting tools. The austenite decomposes into different product phases depending on the rate of cooling history. Consequently, in order to realistically simulate the forming and cooling process of hot stamping, an FE model based on the metallo-thermo-mechanical coupling theory is very important (Ref 13). In order to realistically predict the hot stamping process of TWBs, information on the boron-manganese steel B1500HS, the joint partner B340LA, and the welding zone, including the heat-affected zone (HAZ), should be sufficiently accurate to describe thermal, mechanical, and metallurgical parameters. In addition to various elastic and plastic material parameters, in order to describe the material behavior during forming, the heat transfer coefficient in forming processes at elevated temperatures, phase transformation modeling, and the definition of the flow stress as a function of strain, strain rate, and temperature are essential in order to achieve reliable simulation results. In this article, modeling and simulation of hot stamping tailor-welded high-strength steels, including phase transformation modeling, thermal modeling, and thermal-mechanical modeling is investigated. In addition, the results obtained from the numerical simulations are analyzed and critically compared with experimental results. Finally, the obtained results such as Vickers hardness, microstructure distribution, and formability of TWBs are highlighted and discussed.

2. Phase Transformation Modeling

Starting with a fully austenitized microstructure, an austenite decomposition model is used to describe the decomposition of austenite into its product phases.

For the diffusion-controlled transformation of austenite into ferrite, pearlite, and bainite, the Johnson-Mehl-Avrami (JMA) equation (Ref 14) is applied for evaluating volume fractions. The equation of diffusion-type transformations can be described as

$$V = 1 - \exp(-bt^n), \quad n = \frac{\ln\left[\frac{\ln(1-V_1)}{\ln(1-V_2)}\right]}{\ln\left(\frac{t_1}{t_2}\right)}, \quad b = -\frac{\ln(1-V_1)}{t_1^n}, \tag{Eq 1}$$

where t_1 and t_2 are the isothermal time of certain temperature and V_1 and V_2 are the volume fractions of phase transformations at certain temperature, which in turn depend on time-temperature transformation (TTT) curves of the selected steel. For the diffusion-type transformation, the incubation period and the phase transformation volume fractions can be determined according to Scheil's additivity method (Ref 15).

Åkerström and Oldenburg (Ref 16) modified the rate equation of phase transformation by Kirkaldy and Venugopalan (Ref 17) to account for the effect of boron. The decomposition of austenite into the product phases ferrite, pearlite, and bainite is described using the differential equation:

$$\frac{dX_j}{dt} = f_1(T)f_2(C)f_3(G)f_4(X_j), \tag{Eq 2}$$

where X_j are the so-called ghost fractions. Accordingly, the value for the ghost fractions X_j varies between 0 and 1. $f_1(T)$ is a function of temperature, describing the temperature dependence of the reaction rate. $f_2(C)$ is the effect of alloy composition. $f_3(G)$ is the effect of the austenite grain size, where G is the ASTM grain size number for the austenite. In this work, a constant austenite grain size is assumed during cooling. $f_4(X_j)$ takes into account the current amount of the different phases.

The volume fraction of non-diffusion type transformation only depends on temperature, and is not sensitive to cooling rate. Regardless of the effect of stresses on non-diffusion type transformation, Koistien and Marburger (Ref 18) described the equation of non-diffusion type transformation as the function of temperature:

$$X_m = X_\gamma(1 - \exp(-\alpha(M_s - T))), \tag{Eq 3}$$

where X_m is the current fraction of martensite, $X\gamma$ is the volume fraction of remaining austenite, M_s is the martensite start temperature, and α is a constant and can be used to control the velocity of the martensitic transformation. Usually, α assumes values between 0.011 and 0.033.

Hardness distribution is calculated using empirically based equations as a function of steel composition and cooling rate. Maynier et al. (Ref 19) presented the computation model evaluating the hardness of ferrite, pearlite, bainite, and martensite.

In case of martensite phase, the hardness computation model is presented as

$$\mathrm{HV_M} = 127 + 949\mathrm{C} + 27\mathrm{Si} + 11\mathrm{Mn} + 8\mathrm{Ni} + 16\mathrm{Cr} + 21\log V_r, \tag{Eq 4}$$

where $\mathrm{HV_M}$ is the Vickers hardness of martensite; V_r is the cooling rate at 700 °C; and C, Si, Mn, Ni and Cr are the percentage of steel compositions, respectively.

For bainite phase, the hardness computation model is presented as

$$\begin{aligned}\mathrm{HV_B} = {} & 323 + 185\mathrm{C} + 330\mathrm{Si} + 153\mathrm{Mn} + 65\mathrm{Ni} + 144\mathrm{Cr} \\ & + 191\mathrm{Mo} + (89 + 53\mathrm{C} - 55\mathrm{Si} - 22\mathrm{Mn} - 10\mathrm{Ni} - 20 \\ & \mathrm{Cr} - 33\mathrm{Mo})\log V_r\end{aligned} \tag{Eq 5}$$

Variable definitions are similar as in Eq 4.

For pearlite and ferrite phases, the hardness computation model is presented as

$$\begin{aligned}\mathrm{HV_{F-P}} = {} & 42 + 223\mathrm{C} + 53\mathrm{Si} + 30\mathrm{Mn} + 12.6\mathrm{Ni} + 7\mathrm{Cr} + 19\mathrm{Mo} \\ & + (10 - 19\mathrm{Si} + 4\mathrm{Ni} + 8\mathrm{Cr} + 130V)\log V_r\end{aligned} \tag{Eq 6}$$

Variable definitions are similar as in Eq 4.

The hardness of steel is the weighted arithmetic mean of every phase. It can be evaluated by the following equation:

$$\mathrm{HV} = \xi_M\mathrm{HV_M} + \xi_B\mathrm{HV_B} + (\xi_F + \xi_P)\mathrm{HV_{F+P}}, \tag{Eq 7}$$

where HV is the Vickers hardness of steel. ξ_M, ξ_B, ξ_F, and ξ_P are the volume fractions of martensite, bainite, ferrite, and pearlite, respectively.

3. Thermal Modeling

For the quality of the formed TWBs, it is important to guarantee a homogeneous martensitic microstructure in boron material regions, and therefore numerical simulations should

model and predict with a great accuracy the physical mechanisms of heat transfer.

During the transfer process from the furnace to the die, the blank temperature is reduced due to convection and radiation. Convection heat transfer coefficient is strongly affected by Reynolds number (Re) and Richardson number (Ri) (Ref 20). In thermal convection problems, Reynolds number is the ratio of inertial forces to viscous forces, while Richardson number represents the importance of natural convection relative to the forced convection. Some empirical correlations will be proposed to improve calculation accuracy. The radiation shape factor is the most important parameter for radiation coefficient. The radiation shape factor from the upper surface of the blank to the bottom surfaces of the punch and the blank holder can be adopted from Ref 16. In this case, the radiation heat transfer coefficient is variable during the process and depends on the distance between the blank and die. The heat transfer with the environment was defined as a function of the temperature as reported in Åkerström and Oldenburg (Ref 16).

The convection heat transfer follows Newton's law of cooling

$$Q_{\text{conv}} = H_{\text{k}}(T_{\text{b}} - T_{\text{c}}), \quad \text{(Eq 8)}$$

where T_{b} is the blank temperature. In this model, $H_{\text{k}} = 17\ \text{W}/\text{m}^2\text{K}$.

The radiation heat transfer to environment was modeled using the Stefan-Boltzmann law

$$\text{Q}_{\text{Rad}} = \varepsilon\sigma\left(T_{\text{b}}^4 - T_{\text{c}}^4\right), \quad \text{(Eq 9)}$$

where σ is Stefan-Boltzmann constant which equals 5.669×10^{-8} and ε is the emissivity which directly depends on the surface type. In this model, ε =0.8 was used (Ref 21), as there is an oxidized surface on the blank sheet.

During the forming and quenching process, the hot blank is cooled down mainly by contact heat transfer. Equation 10 shows the relationship for heat transfer between dies and blank:

$$Q_{\text{cont}} = \text{HTC}(T_{\text{b}} - T_{\text{c}}), \quad \text{(Eq 10)}$$

where HTC is the contact conductance. Contact conductance is related to temperature, material, and pressure. The analytical model of contact conductance for specific boron steel was established. Inverse simulations and nonlinear regression analysis are used to determine a general model of the interfacial heat transfer coefficient in the hot stamping process in different contact conditions. The different contact conditions studied are mechanical contact at different contact pressures and contact at a thin air gap between the hot blank and cold tool. In the inverse simulation, a thermo-mechanical coupled finite element model is used with a thermo-elastic-plastic constitutive model, including effects from changes in the microstructure during quenching.

HTC as a function of the contact pressure (p) can be linearly fitted as

$$\text{HTC}(p) = 59 * p + 1224 \ \left[\text{W}/\text{m}^2\text{K}\right], \quad \text{(Eq 11)}$$

where p is given in MPa, for $0 \le p \le 50$ MPa, and $\text{HTC}(p) = \text{HTC}(50) = 4174\ [\text{W}/\text{m}^2\text{K}]$ for $p > 50$ MPa, which is a slightly different from $\text{HTC}(p) = 53.4 * p + 1316\ [\text{W}/\text{m}^2\text{K}]$ according to the work of Lechler et al. (Ref 22).

For the FE analysis of hot stamping TWBs, the thermal conditions of not only the boron steel but also the joint partner HSLA steel should be represented. It was found that the heat conductance of the two partner materials was almost the same (Ref 22), which simplified the analysis significantly. In the article, the heat conductance of boron steel is adopted as the input parameter for HSLA steel.

As the percentage of the weld zone surface is negligible compared to the total remaining boron steel and HSLA steel, no specific heat transfer coefficient for the seam area was taken.

4. Thermo-mechanical Modeling

During hot stamping process, the influence of temperature and strain rate has to be taken into account in order to describe

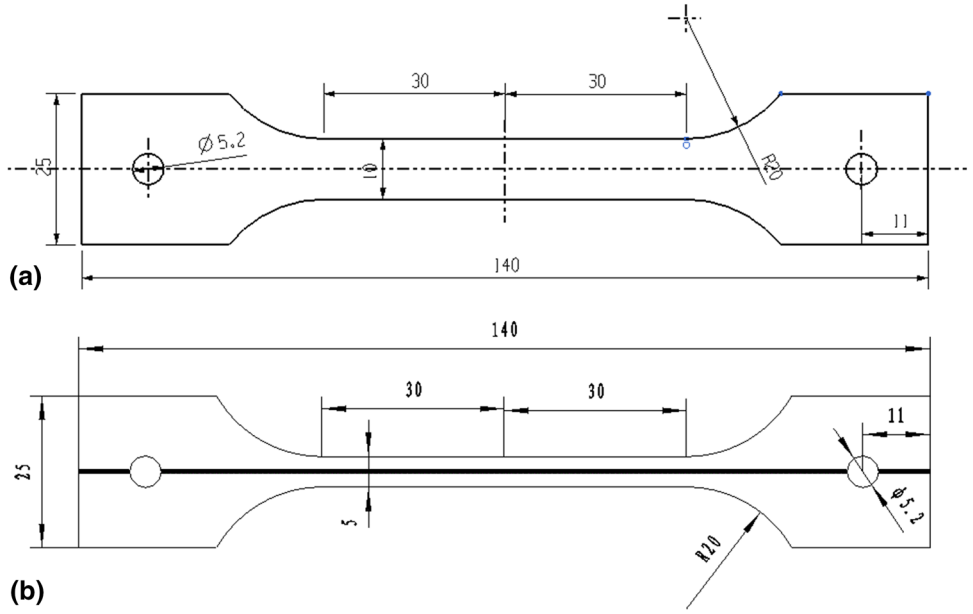

Fig. 1 Schematic sketch for the analysis of flow behavior at elevated temperatures: (a) base material and (b) weld seam

the material rheological behavior, which is necessary to carry out FE simulation (Ref 12).

1.2-mm-thick B340LA sheet and 2.0-mm-thick B410LA sheet are, respectively, butt welded with 1.6-mm-thick B1500HS sheet by German IPG fiber laser machine. Detailed process parameters can be found in Ref 12. The tailor-welded sheet metal is divided into three zones: base material B1500HS, base material B340LA, and weld seam. In order to obtain a reliable and accurate rheological behavior description model, tensile specimens of base material and weld seam, shown in Fig. 1 and 2, respectively, are used to evaluate the flow behavior of base material and weld seam at elevated temperatures. The tensile test specimen in Fig. 1(b) is 5 mm wide, consisting of the narrow weld ($b \approx 2$ mm) in the middle, HAZ, and the two basic materials B1500HS and B340LA.

Thermo-mechanical Simulator—Gleeble® 1500 is used to investigate the forming behavior of base materials and weld seam. The tensile specimen is heated to 950 °C and maintained for 5 min for complete austenitization. Then the specimen is cooled down to test temperature using compressed air, followed by hot tensile tests at a constant temperature between 500 and 800 °C and with different strain rates of 0.05, 0.1, 1.0, and 10.0 s^{-1} to determine the flow stress curves. The tensile tests at a given temperature and strain rate are repeated three times because of experimental instability, and the averaged stress-strain curves at a strain rate of 0.1 s^{-1} as an example are plotted in Fig. 3. It is apparent that the hardening behavior of base material and weld seam is highly temperature sensitive. When

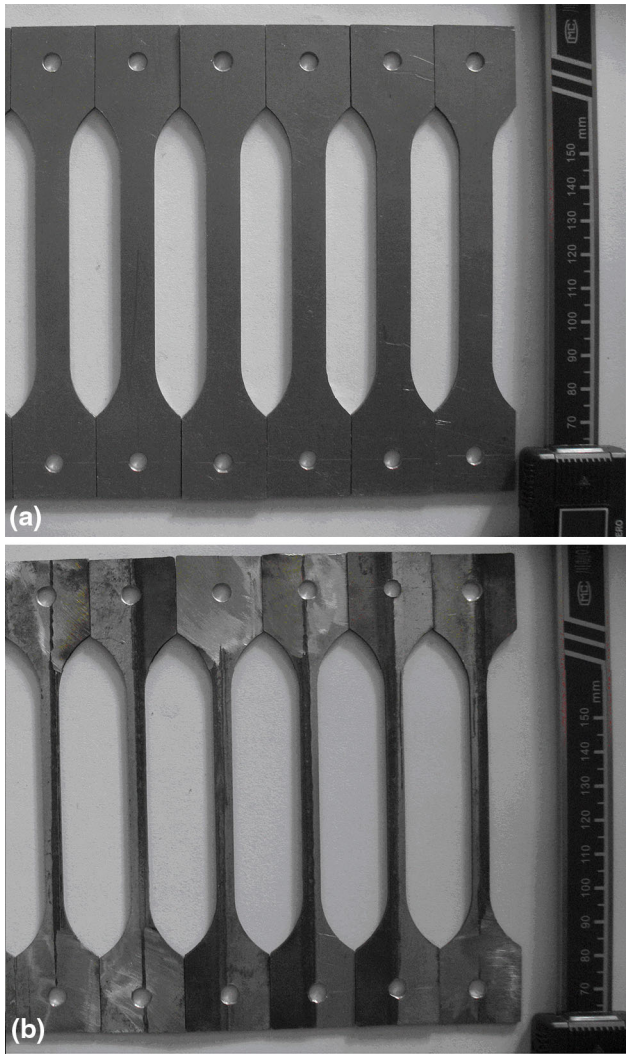

Fig. 2 Tensile specimens for the analysis of flow behavior at elevated temperatures: (a) base material and (b) weld seam

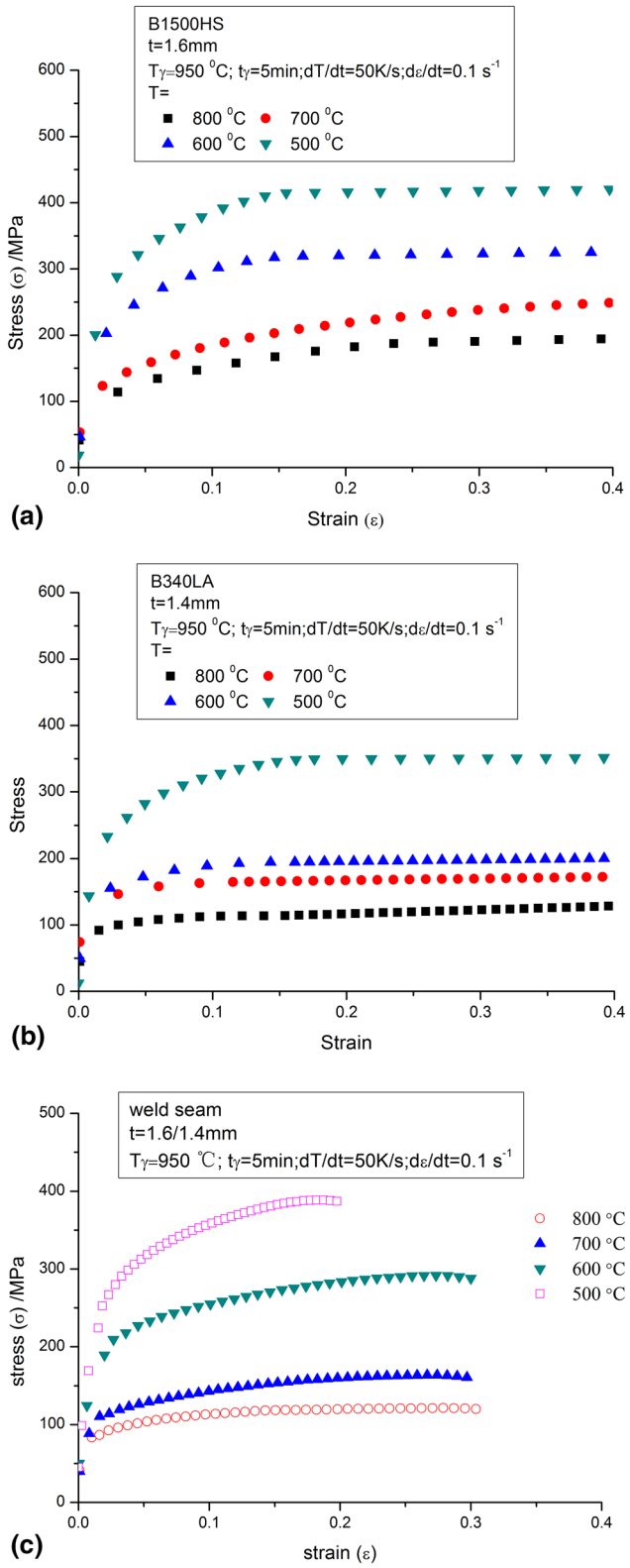

Fig. 3 Flow curves at elevated temperatures depending on the temperature: (a) B1500HS, (b) B340LA, and (c) weld seam

the temperature increases from 500 to 800 °C, the reduction of yield stress of B340LA is much higher than that of B1500HS, which shows that B340LA is more sensitive to temperature than B1500HS.

The effect of temperature on the flow properties of the weld seam of material B1500HS and B340LA is shown in Fig. 3(c). The results show that with the increase of temperature, the yield stress begins to reduce, which is due to a thermally activated increase of the dislocation movements (Ref 23). At lower temperature, 500 °C for an instance, the flow stress of material B1500HS, B340LA, and weld seam shows a similar tendency with a maximum tensile stress of about 400 MPa. With the increase of temperature, the flow stress of material B340LA drops significantly compared with that of material B1500HS and weld seam, showing relatively higher formability at elevated temperature.

The flow curves in Fig. 4 show that the flow stress of material B1500HS and B340LA is obviously sensitive to strain rate, except for the case of strain rates of 0.1 and 0.05 s^{-1}. The reason for the phenomenon could be explained that at lower strain rate, the flow behavior of boron steel B1500HS and HSLA steel B340LA is not sensitive to strain rate.

Hot tensile tests of the weld seam are carried out at various temperatures with different strain rates. As illustrated in Fig. 4(c), the studies on the effect of strain rate on the flow behavior of the weld zone in case of elevated temperature of 800 °C show that the plastic deformation behavior of the weld seam is significantly dependent on strain rate.

Figure 5 shows the stress-strain curves of the 5-mm-wide seam along with the joint partners of the two base materials B1500HS and B340LA at 600 °C and with a strain rate of 0.1 s^{-1}. The results show that the flow curve of the weld seam is above that of alloyed steel B340LA, but below the one of boron-manganese B1500HS.

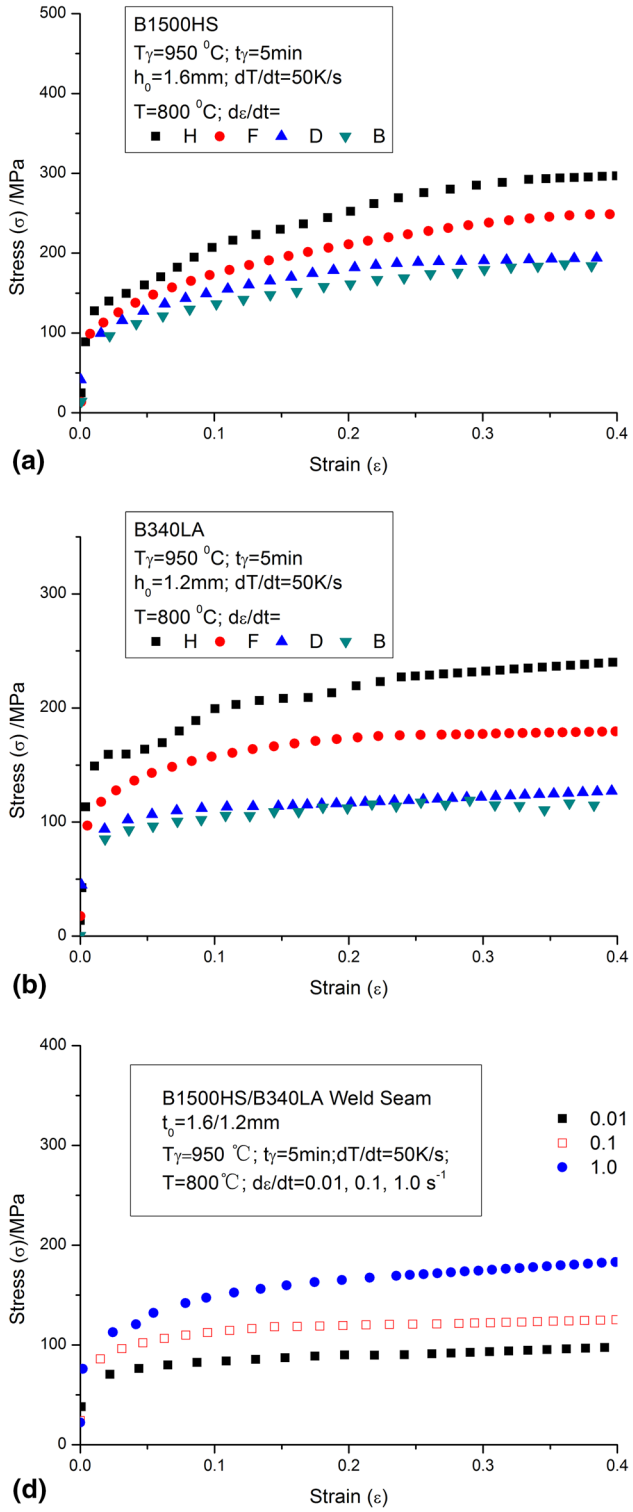

Fig. 4 Flow curves at elevated temperatures depending on the strain rate: (a) B1500HS, (b) B340LA, and (c) weld seam

5. Experiment and Simulation Results

5.1 Experimental Results of TWBs Hot Stamping

Figure 6(a) shows the die set which is composed of upper punch, lower die, and blank holder. Tailor-welded high-strength steels with two kinds of weld seam locations were chosen for the experiment. As shown in Fig. 6(b), boron steel B1500HS is tailor welded on the top of the blank, where exhibited resistance to deformation. In order to achieve softer mechanical properties after quenching process, HSLA steel B340LA is tailor welded with B1500HS, functionally acting as energy absorption. In

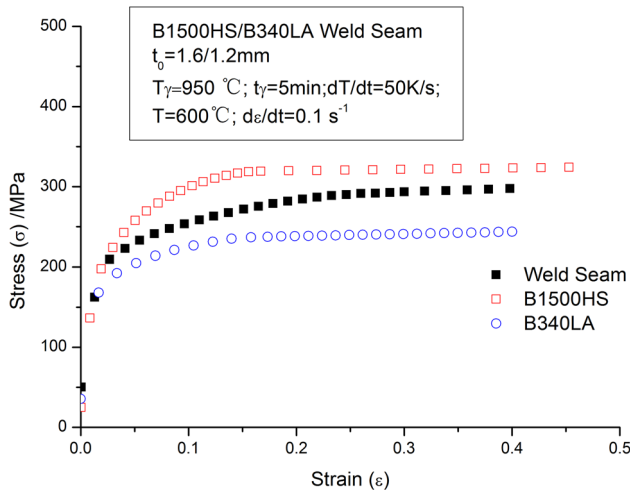

Fig. 5 Flow curves at elevated temperatures depending on the cooling rate: (a) B1500HS and (b) B340LA

Fig. 6(b), two samples are intended to show the movement of different locations of weld seam, and to find the weakest zone at different locations with differently located weld seam. In this way, an automobile component mini b-pillar can be manufactured with functionally optimized and tailored mechanical properties.

The designed tool was continuously cooled using chilled water recirculation and maintained at room temperature. The blanks were heated to 950 °C for complete austenitization and then transferred from the furnace to the tool in 5-7 s and subjected to contact pressure during closure for controlled cooling. The punch moved down with a speed of 40 mm/s and the workpiece was deformed. Afterward, it was quenched in the die and maintained for 10 s.

Figure 7 shows the hot stamped mini b-pillar using TWBs, where SN represents weld seam including heat-affected zone. The fracture does not appear in the product, but there is strong wrinkle tendency in the binder area, where the flat blank came into contact with the blank holder. The reason for the significant wrinkle tendency is that there is a 2 mm clearance between binder and die face, aiming to reduce the contact pressure and consequently decrease the heat transfer between them.

Hardness and microstructure of two base materials and the region near weld seam location were observed in order to investigate the mechanical properties. The location of test specimen is presented in Fig. 7 and the hollow arrow shows the measuring direction, ranging from −4 to 4, where −4 and 4 means the start and ending position of measuring points, respectively.

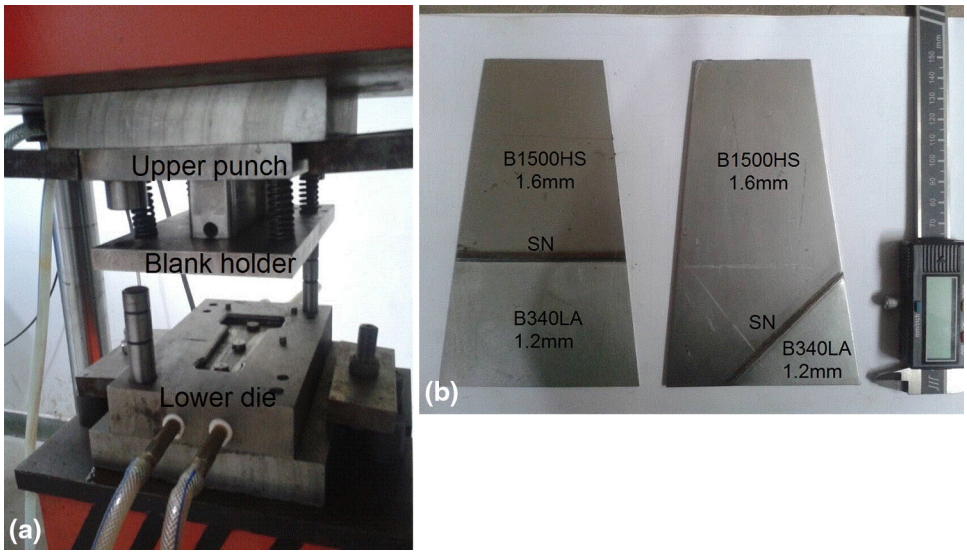

Fig. 6 Experimental apparatus and initial flat blanks: (a) die set and (b) initial flat blanks

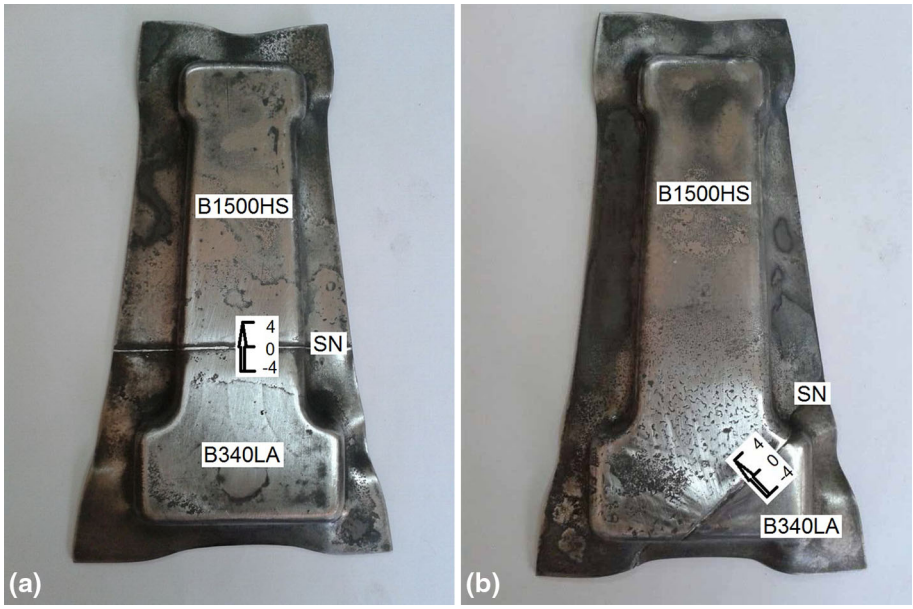

Fig. 7 Hot stamped mini b-pillars: (a) with weld seam SN-A and (b) with weld seam SN-B

Microstructure distribution at locations before and after hot stamping is illustrated in Fig. 8. The as-received microstructure of B1500HS shows anisotropic inhomogeneity observed as the secondary microstructural banding of ferrite-pearlitic steel. The anisotropic character was caused by cold rolling process and the grains are oriented in the rolling direction. In the as-received state, it is easy to find that the main structure of B340LA is predominately ferrite with a small amount of

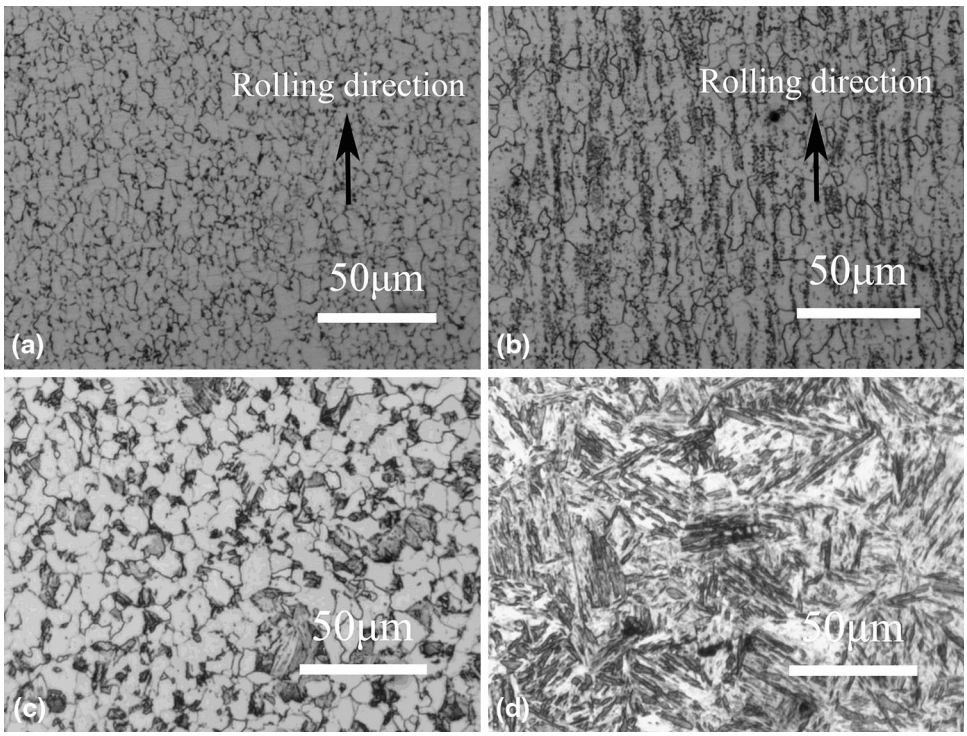

Fig. 8 Microstructure before and after hot stamping: (a) B340LA before hot stamping, (b) B1500HS before hot stamping, (c) B340LA after hot stamping, and (d) B1500HS after hot stamping

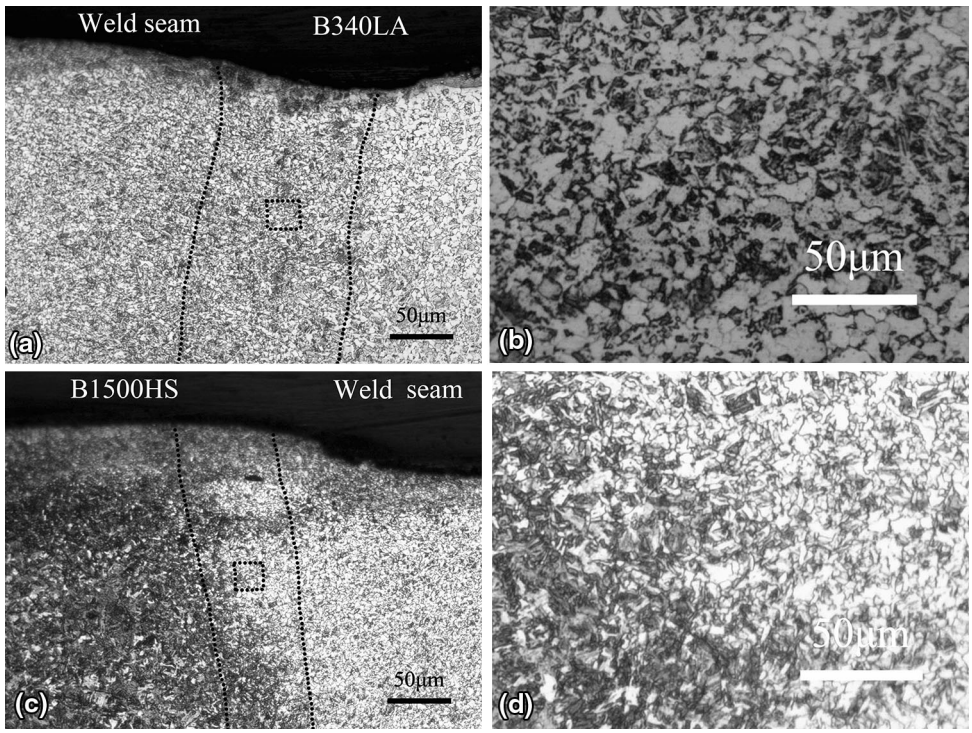

Fig. 9 Microscopy images of transitions of weld seam and base material: (a) B340LA and weld seam, (b) partial enlarged image, (c) B1500HS and weld seam, and (d) partial enlarged image

pearlite. Similar to B1500HS, microstructure in the B340LA side shows anisotropic inhomogeneity because of cold rolling process.

For the base metal B340LA, the microstructure after hot stamping process is retained as a mixture of ferrite and pearlite, with equiaxed grains scattered uniformly, which leads to lower anisotropic inhomogeneity. After hot stamping, the Vickers hardness at the upper side of base metal B1500HS is about 490HV, which shows that the microstructure at the upper side of the base metal B1500HS is fully martensite. The Vickers hardness at the side wall is as low as 450HV, which shows that the microstructure at the side wall is a mixture of bainite and martensite. This can be explained by the reduced contact pressure along the walls, which leads to the reduced cooling rate and also the deformation during quenching. It shows that the deformation during quenching can cause the shift in the CCT diagram and allows bainite formation (Ref 24).

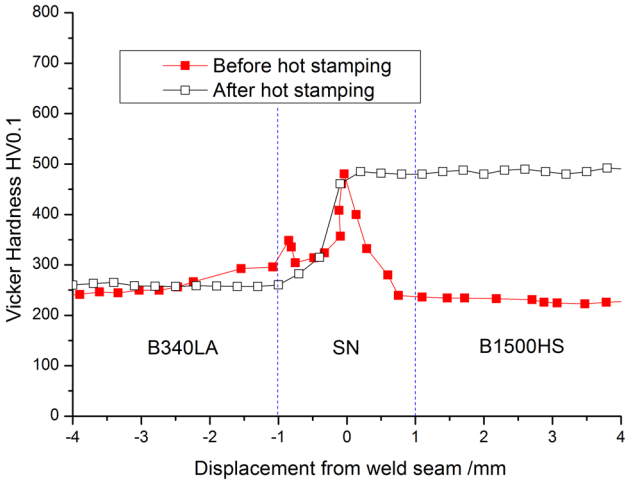

Fig. 10 Microhardness distributions perpendicular to weld seam before and after hot stamping process

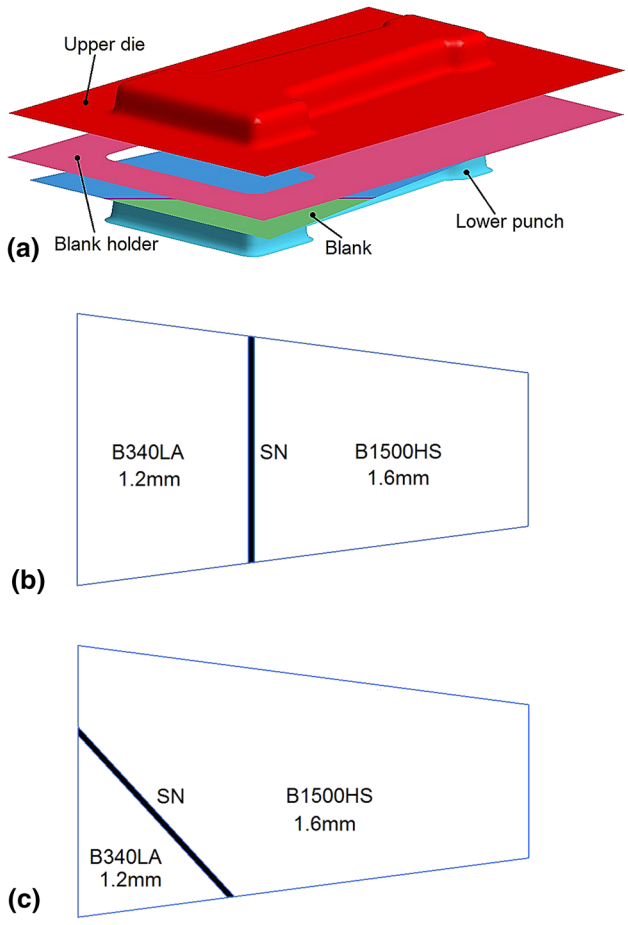

Fig. 11 FE analysis model and contour of initial flat blank: (a) FE model, (b) blank contour with weld seam SN-A, and (c) blank contour with weld seam SN-B

The transitions between base materials B340LA and B1500HS and weld seam are shown in Fig. 9. Figure 9(b) and (d) are partially enlarged images of the dotted BOX shown in Fig. 9(a) and (c), respectively. It can be concluded that the transition zone is continuous and narrow, guaranteeing a sharp and uniform transition of mechanical properties from base material to weld seam.

The width of weld seam including HAZ is about 2 mm. As the HAZ is very narrow compared to the dimension of flat blank, it is regarded as one part of weld seam in the paper. The sharp hardness gradient in the weld seam before hot stamping is due to a martensitic structural transformation on the side of the boron steel B1500HS due to high cooling rates of the welding process (Ref 25). There is an uneven increase in the hardness profile across the weld illustrated in Fig. 10. The detected hardness drop in the center of the weld is due to a lower cooling rate in the welding process, compared to the adjacent area to the base materials.

Figure 10 shows the Vickers hardness distributions after quenching process over the cross section of the weld seam. The Vickers hardness of the weld seam increases continuously and immediately from soft base material B340LA to hardened base

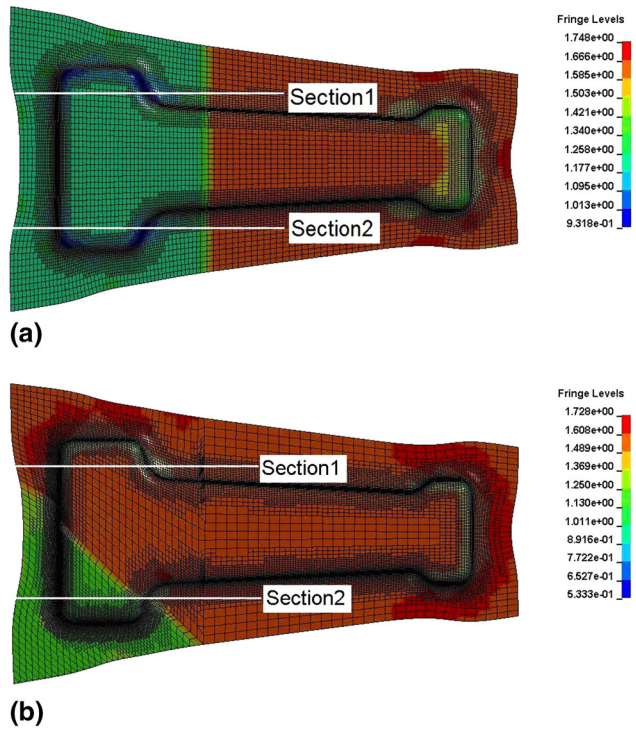

Fig. 12 Thickness distribution and cutting sections: (a) with weld seam SN-A and (b) with weld seam SN-B

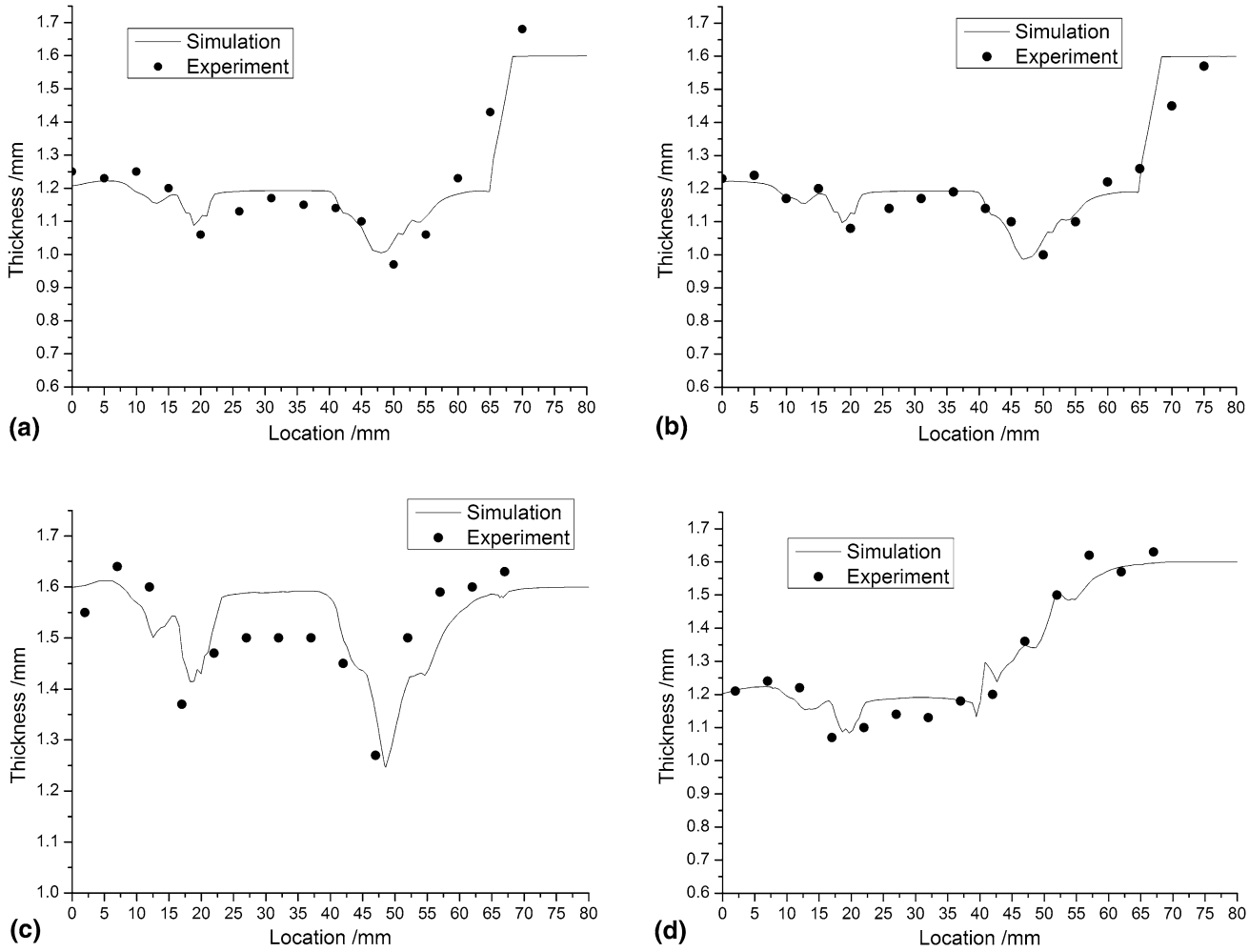

Fig. 13 Thickness distribution comparisons between experimental and simulation results: (a) section 1 with weld seam SN-A, (b) section 2 with weld seam SN-A, (c) section 1 with weld seam SN-B, and (d) section 2 with weld seam SN-B

material B1500HS. The results in Fig. 13 show that the Vickers hardness of boron-manganese steel B1500HS after quenching process is about 500 HV0.1, which is twice more than the hardness in the as-received state of 200 HV0.1. It is shown that the Vickers hardness of micro-alloyed steel B340LA experiences a minor increase after hot stamping, rising from 170 to 200 HV0.1. The reason for the increase of hardness is probably due to the fact that B340LA experiences recovery, recrystallization, and grain growth, the grains in turn undergoing a columnar-to-equiaxed grain shape transition. The significantly heterogeneous hardening of the weld zone is about 400 HV0.1 which is about twice the hardness of the partner material B340LA. The desired ultimate tensile strength is 500-665 MPa, and the corresponding hardness value is about 150 HV0.1 to 200 HV0.1. The Vickers hardness of the partner material B340LA before and after hot stamping shows that it meets the requirements quite well.

5.2 Numerical Simulation of TWBs Hot Stamping

The mini b-pillar is used for FE simulation, for the evaluation of the forming behavior of hot stamping tailor-welded blanks of base material B1500HS and joint partner B340LA. Figure 11(a) shows the FE analysis model which consists of blank, upper die, lower punch, and blank holder. The dynamic explicit code LS-DYNA is used and FE analysis is performed where both forming and heat transfer are simultaneously solved. *MAT_244, which is based on the work done by Akerstrom (Ref 16), was mainly suited for hot stamping processes where phase transformations are crucial and was used as a model of the boron steel B1500HS. Since there is no phase transformation during forming and quenching process for base material B340LA, *MAT_106, which is an elastic-viscoplastic material with thermal effects, was used as a model. Details of the chemical compositions of the investigated materials can be found in (Ref 12). Flow curves as a function of strain, temperature, and strain rate have been obtained by tensile tests at elevated temperatures. A contact heat transfer coefficient based on the contact pressure was used in the simulation. Friction coefficient was regarded as a constant value 0.35 (Ref 26). The forming limit diagrams (FLDs) of the base materials and welded zone were evaluated on the experimentally obtained forming limit curves (FLCs) using similar steel brands (Ref 27).

In Fig. 11(b) and (c), the left side of weld seam is B340LA and the right is B1500HS. Two weld seam locations in the mini b-pillar are selected in order to comprehensively analyze the

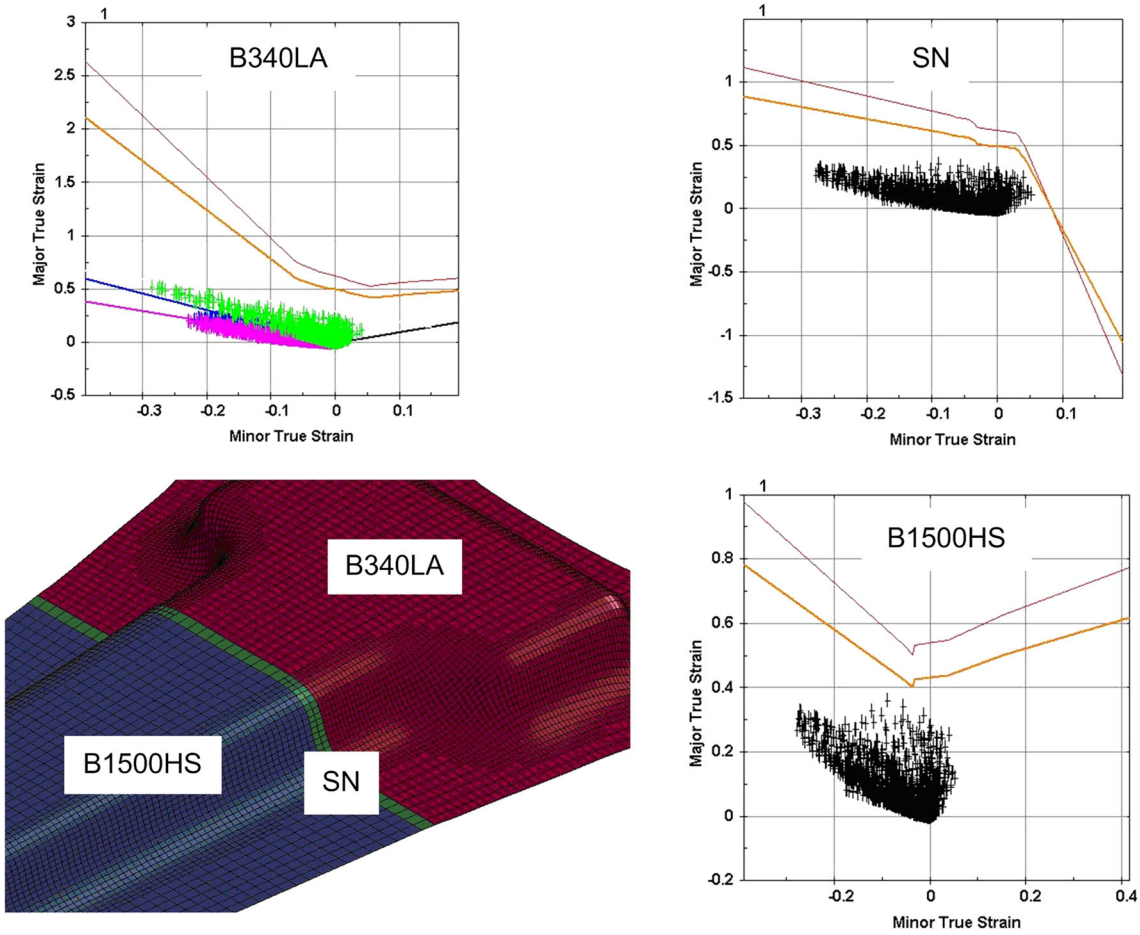

Fig. 14 FLDs of hot stamped mini b-pillar with weld seam SN-A

forming and failure properties of TWBs' hot stamping based on the position of the weld seam in the initial flat blank. The weld seams are represented by lines SN-A and SN-B, respectively. The base material and weld seam in FE model are discretized with 5050 quadrilateral shell elements. Adaptive mesh refinement technology is used in the FE model during hot stamping simulation.

Thickness distribution of hot stamped mini b-pillar with two weld seams is shown in Fig. 12. It shows that the minimum thickness value is located in the filleted corner of the B340LA side. The maximum value is located in the binder area, where the flat blank came into contact with the blank holder. The reason is that there is 2 mm clearance between the die face and the blank holder, which is bigger than the sheet thickness, leading to significant wrinkle tendency. In order to show the thickness distribution clearly and verify the reliability of FE simulation, two section cuts are schematically shown in Fig. 12.

Figure 13 shows thickness distribution along different cutting sections. There is an obvious thickness variation at the die radius near the filleted corners. The comparisons between simulation and experiment results show that the numerical data agree well with the experimental results and the currently used thermo-mechanical model can well reflect the deformation strategy during hot stamping process.

Figure 14 illustrates the formability of mini b-pillar with weld seam SN-A during hot stamping. Formability at each region, i.e., B340LA and B1500HS base metal and weld seam, is evaluated by using FLDs. No cracks are seen in the formed material, while minor wrinkles appear at the thinner side. As mentioned before, there is a 2 mm clearance between die face and binder, resulting in weak flow resistance at the thinner side. Furthermore, defects such as weld line movement and subsequent fracture at the region near weld line does not appear. The reason for this is that the weld line is perpendicular to the forming direction, in order to prevent deformation at the weld region.

The deformation path of critical regions of hot stamped mini b-pillar with SN-B is shown in Fig. 15. It shows that elements of B340LA near weld seam are at a risk of cracking, while elements of weld seam and base steel B1500HS remain safe. It can be concluded that even when the base material is beyond its formability extreme, the weld seam remains safe. Neither of the investigated weld seam positions initiates failure and crack in the weld seam nor does in the HAZ. Even for the case of SN-B, where the weld seam is coming through the critical area, failure and crack initiation were not observed in the weld seam and HAZ.

The results show that all the failure is related to the base materials, and it can be concluded that the formability of hot stamping TWBs is limited to the formability of the joint partners. Lechler et al. (Ref 11) have verified also that, under mass production conditions, failure of hot stamped tailor-welded blanks could only be observed in typical forming in

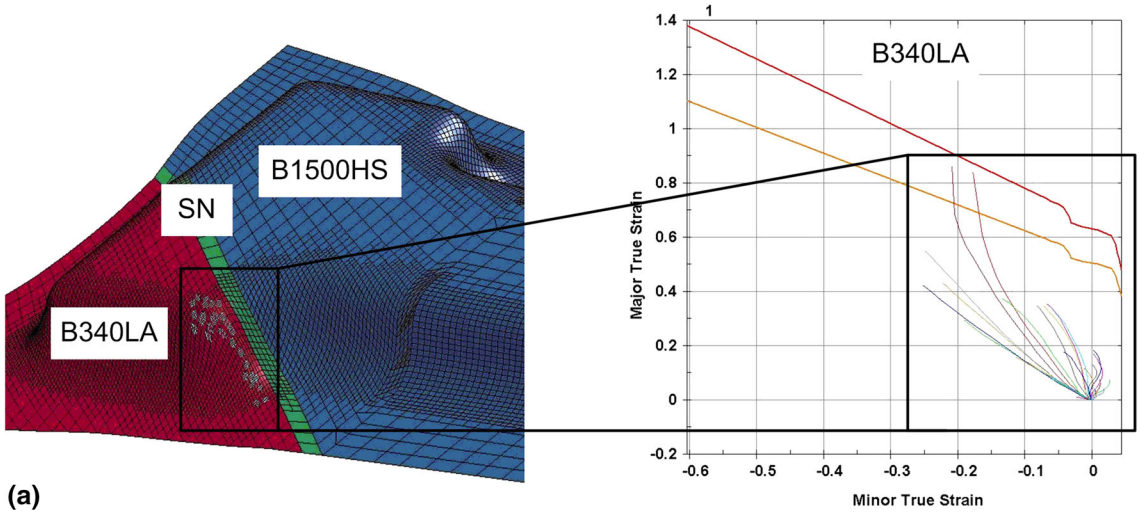

(a)

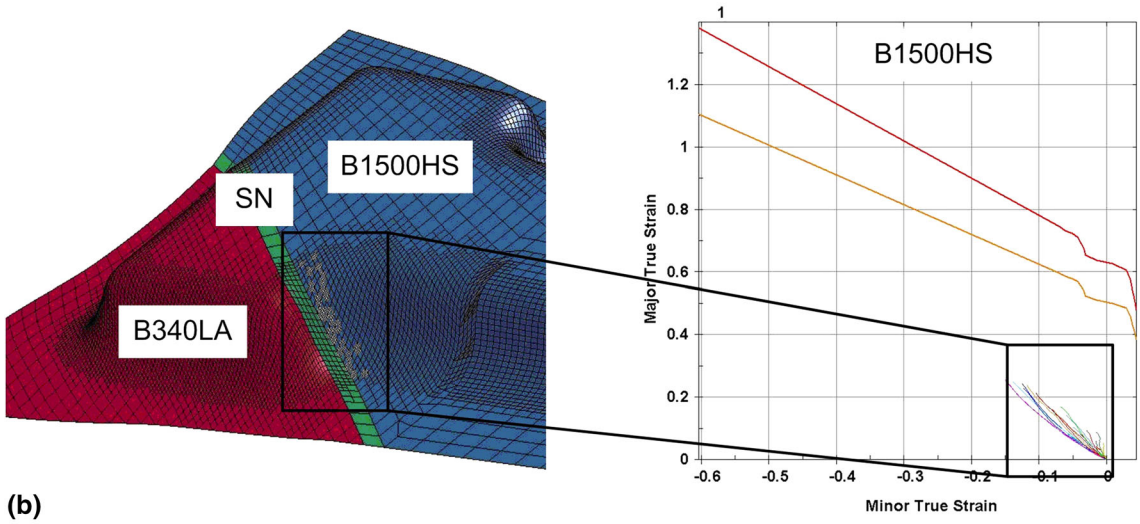

(b)

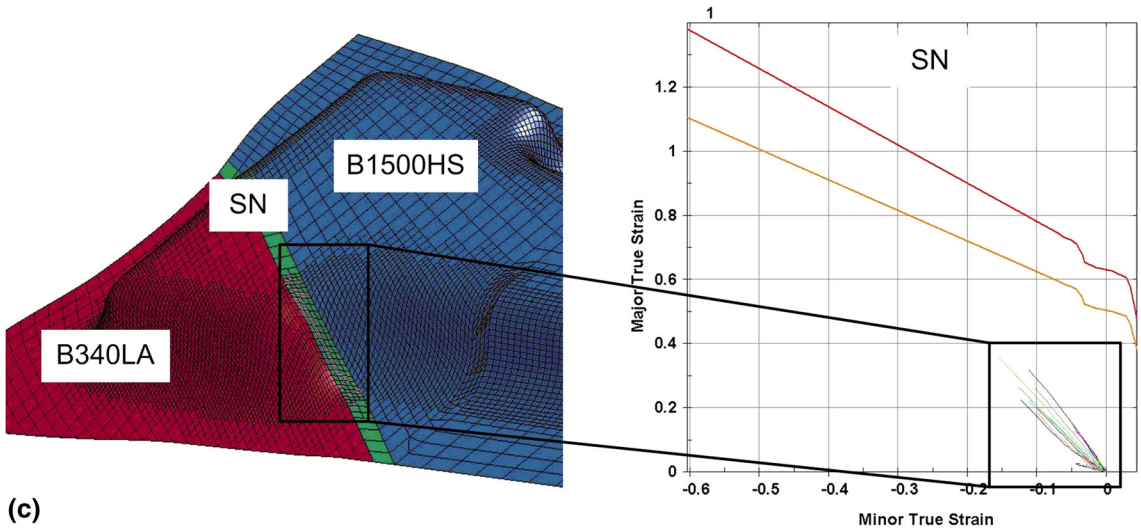

(c)

Fig. 15 FLDs of hot stamped mini b-pillar with weld seam SN-B: (a) B340LA, (b) B1500HS, and (c) SN

critical areas in the flange and the edge radii of one of the two base materials.

6. Conclusions

Hot stamped mini b-pillar has been developed by tailor-welded high-strength steels for the light-weight construction and high crash performance.

(1) In order to carry out FE simulation of hot stamping process, thermal, mechanical, and metallurgical aspects of base material B1500HS, B340LA, and weld seam were theoretically and experimentally analyzed.
(2) As a result of hot stamping experiment using TWBs, a mini b-pillar can be manufactured without fracture and wrinkling. The experiment results show that the hardness is somewhat reduced at the side wall as compared to that at the upper region due to the reduced contact pressure that affects strongly cooling rate. The FLDs of the simulation results show that the FE model can well reflect the formability of base material and weld seam. Even though forming limit of base materials B1500HS and B340LA is slightly higher than that of weld seam, there is no evidence showing that the weld seam has a slightly poor formability. The fact is that when the base material approaches the forming limit, there is still some margin for the weld seam.
(3) Comparisons between the experimental and simulation results confirm that the numerical model is able to accurately predict the formability and the material flow during hot stamping process.

Acknowledgments

The support of the National Natural Science Foundation of China (Nos. 51005137, 51375280), the Program for New Century Excellent Talents in University (NCET-12-1028), the Shandong Provincial Natural Science Foundation (No. ZR2013EEZ003), the Shandong Provincial Key R&D Program (No. 2015GGX103029), and the Doctoral Foundation of Shandong Jianzhu University (No. XNBS1243) is gratefully acknowledged.

References

1. T. Labudde and W. Bleck, Formability Characterization of Press Hardening Steels, *2nd International Conference Hot Sheet Metal Forming of High Performance Steel*, M. Oldenburg, K. Steinhoff, B. Prakash, Eds., June 15-17, 2009 (Luleå), Verlag Wissenschaftliche Scripten, 2009, p 127–135
2. A.E. Tekkaya, H. Karbasian, W. Homberg, and M. Kleiner, Thermo-mechanical Coupled Simulation of Hot Stamping Components for Process Design, *Prod. Eng. Res. Dev.*, 2010, **1**, p 85–89
3. P. Hein and J. Wilsius, Status and Innovative Trends in Hot Stamping of USIBOR 1500 P, *Steel Res. Int.*, 2008, **79**(2), p 85–91
4. M. Maikranz-Valentin, U. Weidig, U. Schoof, H.H. Becker, and K. Steinhoff, Components with Optimised Properties due to Advanced Thermo-mechanical Process Strategies in Hot Sheet Metal Forming, *Steel Res. Int.*, 2008, **79**(2), p 92–97
5. J. Banik, F.-J. Lenze, S. Sikora, R. Laurenz, Tailored Properties—A Pivotal Question for Hot Forming, *3rd International Conference Hot Sheet Metal Forming of High-Performance Steel*, M. Oldenburg, K. Steinhoff, B. Prakash, Eds., June 13-16, 2011 (Kassel), Verlag Wissenschaftliche Scripten, 2009, p 13–20
6. B.T. Tang, Q.L. Wang, S. Bruschi, A. Ghiotti, and P.F. Bariani, Influence of Temperature and Deformation on Phase Transformation and Vickers Hardness in Tailored Tempering Process: Numerical and Experimental Verifications, *J. Manuf. Sci. T ASME*, 2014, **136**(5), p 051018-1–051018-14
7. B. Casas, D. Latre, N. Rodríguez, I. Valls, Tailor Made Tool Materials for the Present and Upcoming Tooling Solutions in Hot Sheet Metal Forming, *1st International Conference Hot Sheet Metal Forming of High-Performance Steel*, K. Steinhoff, M. Oldenburg, B. Prakash, Eds., Oct 22-24, 2008 (Kassel), GRIPS media, 2008, p 23–36
8. K. Mori and Y. Okuda, Tailor Die Quenching in Hot Stamping for Producing Ultra-High Strength Steel Formed Parts Having Strength Distribution, *CIRP Ann. Manuf. Technol.*, 2010, **59**, p 291–294
9. R. Stopp, L. Schaller, K. Lamprecht, E. Keupp, G. Deinzer, Warmblechumformung in der Automobil-Serienfertigung: status, trends und potenziale, *Tagungsband 2. Erlanger Workshop Warmblechumformung*, M. Geiger, M. Merklein, Eds., Nov 22, 2007 (Erlangen), Meisenbach Verlag, 2007, p 37–58 (**in German**)
10. K. Lamprecht and G. Deinzer, Hot Sheet Metal Forming in Automotive Production, *International Workshop on Thermal Forming and Welding Distortion*, F. Vollertsen, J. Sakkiettibutra, Eds., April 22-23, 2008 (Bremen), BIAS-Verlag, 2008, p 145–154
11. J. Lechler, T. Stöhr, A. Kuppert, M. Merklein, Basic Investigations on Hot Stamping of Tailor Welded Blanks Regarding the Manufacturing of Lightweight Components with Functionally Optimized Mechanical Properties, *Proceeding of NAMRC,* Society of Manufacturing Engineers, Ed., May 26-28, 2010 (Ontario), Curran Associates, Inc., 2010, p 593–600
12. B.T. Tang, Z.J. Yuan, G. Cheng, L.L. Huang, W. Zheng, and H. Xie, Experimental Verification of Tailor Welded Joining Partners for Hot Stamping and Analytical Modeling of TWBs Rheological Constitutive in Austenitic State, *Mater. Sci. Eng. A Struct.*, 2013, **585**(15), p 304–318
13. H. Karbasian and A.E. Tekkaya, A Review on Hot Stamping, *J. Mater. Process. Technol.*, 2010, **210**(15), p 2103–2118
14. A.W. Johnson and R.F. Mehl, Reaction Kinetics in Processes of Nucleation and Growth, *Trans. AIME*, 1939, **135**, p 416–425
15. E. Sheil, Anlaufzeit der Austenitumwandlung, *Arch. Eisenhuettenwes.*, 1935, **12**, p 565–567 (**in German**)
16. P. Åkerström and M. Oldenburg, Austenite Decomposition during Press Hardening of a Boron Steel—Computer Simulation and Test, *J. Mater. Process. Technol.*, 2006, **174**(1–3), p 399–406
17. J.S. Kirkaldy and D. Venugopalan, Prediction of Microstructure and Hardenability in Low Alloy Steels, *International Conference on Phase Transformations in Ferrous Alloys*, A.R. Marder, J.L. Goldstein, Eds., Oct 4-6, 1983 (Philadelphia), Books on Demand, 1983, p 125–148
18. D.F. Koistien and R.E. Marburger, General Equation Prescribing the Extent of Austenite Transformation in Pure Iron-carbon Alloys and Plain Carbon Steels, *Acta Metall.*, 1959, **7**, p 50–60
19. P. Maynier, J. Dollet, P. Bastien, Prediction of Microstructure via Empirical Formulae based on CCT Diagrams, *International Symposium on Hardenability Concepts with Applications to Steels*, D.V. Doane and J.S. Kirkaldy, Eds., 1978 (New York), ASM International, 1978, p 518–544
20. A.M. Clausing, An Experimental Investigation of Natural Convection from an Isothermal Horizontal Plate, *J. Heat Transf. T ASME*, 1989, **111**(4), p 904–908
21. B. Rolfe, A. Abdollahpoor, X.J. Chen, M. Pereira, and N.M. Xiao, Robustness of the Tailored Hot Stamping Process, *Adv. Mater. Res.*, 2015, **1063**, p 177–180
22. J. Lechler, "Beschreibung und Modellierung des Werkstoffverhaltens von presshärtbaren Bor-Manganstählen," Ph.D. Thesis, University of Erlangen-Nuremberg, 2008 (**in German**)
23. B. Wielke, Thermally Activated Dislocation Movement at Plastic Deformation, *Czechoslov. J. Phys. B*, 1981, **31**(2), p 142–156
24. A. Barcellona and D. Palmeri, Effect of Plastic Hot Deformation on the Hardness and Continuous Cooling Transformations of 22MnB5

Microalloyed Boron Steel, *Metall. Mater. Trans. A*, 2009, **40**(5), p 1160–1174

25. H.J. Bargel and G. Schulze, Ed., *Werkstoffkunde*, Springer, Berlin, 2005
26. M. Kerausch, T. Schonbach, Design of Hotforming Processes Based on Sensitivity Analysis of Process Parameters, *Numisheet 2008: the 7th International Conference and Workshop on Numerical Simulation of 3D Sheet Metal Forming Processes*, P. Hora, Ed., Sept 1-5, 2008 (Switzerland), Institute of Virtual Manufacturing, ETH Zurich, 2008, p 563–568
27. M. Merklein, M. Geiger, C.H. Kerausc, J. Lechler, *Presshärten von Tailor Welded Blank (Hot stamping of tailored welded blanks)*, R. Salomon, Ed., 2010 (Düsseldorf), Verlag und Vertriebsgesellschaft mbH, 2010, p 64–68 (**in German**)